*Journal of Ceramic Processing Research. Vol. 20, No. 2, pp. 173~181 (2019)*

J O U R N A L O F
**Ceramic Processing Research**

# $TiCl_3$ and Ni-added Mg prepared by reactive mechanical grinding processing and comparison with $Fe_2O_3$ and Ni-added Mg

**Myoung Youp Song[a,†], Young Jun Kwak[a] and Seong Ho Lee[b]**

[a]*Division of Advanced Materials Engineering, Hydrogen & Fuel Cell Research Center, Engineering Research Institute, Chonbuk National University, 567 Baekje-daero Deokjun-gu, Jeonju 54896, Korea*

[b]*Department of Materials Engineering, Graduate School, Chonbuk National University, 567 Baekje-daero Deokjun-gu, Jeonju 54896, Korea*

**Metallic oxides are brittle and halides have low melting points. They are expected to increase the reaction rates of Mg with hydrogen when added. Samples with compositions of 95 wt% Mg+5 wt% $TiCl_3$ (designated as Mg-5$TiCl_3$), 90 wt% Mg+10 wt% $TiCl_3$ (Mg-10$TiCl_3$), and 80 wt% Mg+14 wt% Ni+6 wt% $TiCl_3$ (Mg-14Ni-6$TiCl_3$) were prepared by high-energy ball milling in hydrogen (reactive mechanical grinding). At the first cycle (n = 1), Mg-5$TiCl_3$ had the highest initial hydrogen uptake rate and the largest quantity of hydrogen absorbed for 60 min at 593 K in 12 bar $H_2$, followed by Mg-10$TiCl_3$ and Mg-14Ni-6$TiCl_3$. Mg-5$TiCl_3$ had an effective hydrogen storage capacity (a quantity of hydrogen absorbed for 60 min) of about 6.3 wt% at n = 1. Mg-5$TiCl_3$ absorbed 4.84 wt% H for 5 min and 6.27 wt% H for 60 min. Decrease in the Mg proportion in Mg-14Ni-6$TiCl_3$, compared with those in Mg-5$TiCl_3$ and Mg-10$TiCl_3$, and the formation of $Mg_2Ni$, with a lower hydrogen storage capacity than Mg, are thought to decrease the initial hydrogen uptake rate and the quantity of hydrogen absorbed for 60 min for Mg-14Ni-6$TiCl_3$. At n = 1, Mg-14Ni-6$TiCl_3$ has the highest initial hydrogen release rate at 593 K in 1.0 bar $H_2$, followed by Mg-10$TiCl_3$ and Mg-5$TiCl_3$. The $Mg_2Ni$ formed in Mg-14Ni-6$TiCl_3$ and the larger content of additives (favoring the nucleation of Mg-H solid solution) are believed to make Mg-14Ni-6$TiCl_3$ have the highest initial hydrogen release rate among these three samples. The hydrogen storage properties of Mg-14Ni-6$TiCl_3$ were compared with those of $Fe_2O_3$ and Ni-added Mg, which were prepared under the conditions similar to those to prepare Mg-14Ni-6$TiCl_3$.**

**Key words: Hydrogen absorbing materials, Phase transition-accompanying milling, Phase transition, Microstructure, $TiCl_3$ or $Fe_2O_3$ addition to Mg.**

## Introduction

Magnesium (Mg) is the most widely studied element for solid-state hydrogen-storage material. By the way, its hydrogen absorption and release rates are low and its hydrogen release temperature is quite high. Many works were performed to increase the hydrogen absorption and release rates of Mg and to increase the hydrogen release temperature of magnesium hydride ($MgH_2$) [1-12].

Ni-added Mg alloys [2, 3] and mechanically-alloyed Mg with Ni under an Ar atmosphere [13-16] increased the hydrogen uptake and release rates of Mg. According to Bobet et al. [17], the hydrogen storage properties of pure Mg and 10 wt% Co, Ni, or Fe-Mg mixtures were improved by milling in planetary ball mill under $H_2$ for a relatively short time of 2 hrs.

Song [13] reviewed the kinetic studies of the hydrogen absorption and release reactions of Mg and reported that the hydrogen absorption and release reactions of Mg are nucleation-controlled under certain conditions and progress by a mechanism of nucleation and growth, and that the hydrogen uptake rates of Mg are controlled by the diffusion of hydrogen through a growing Mg hydride layer.

Oxides of metals are brittle. It is thus expected that addition of oxides of metals to Mg or $MgH_2$ by mechanical grinding can produce defects on the surfaces of and inside the particles and decrease the particle size. Many works were performed to increase the hydrogen absorption and release rates of Mg or $MgH_2$ by grinding Mg mechanically with oxides of metals such as $V_2O_5$ [18, 19], $Cr_2O_3$ [20-22], $Al_2O_3$ [21, 23], $CeO_2$ [21], $Fe_2O_3$ [19, 24], $Fe_3O_4$ [19], $Mn_2O_3$ [19], MgO [25], $La_2O_3$ [26], and $Nb_2O_5$ [27, 28]. During adding some oxides or during hydrogen uptake-release cycling of some oxide-added Mg or $MgH_2$ samples, phase transformation was accompanied. The added oxides could be reduced during milling in hydrogen or hydrogen uptake-release cycling. The $Fe_2O_3$-containing Mg sample hydrided at the 11th cycle contained Fe and a small amount of MgO [24]. This showed that $Fe_2O_3$ was reduced and a small part of Mg was oxidized. The chemical affinity of Mg with oxygen

*Corresponding author:
Tel : +82-63-270-2379
Fax: +82-63-270-2386
E-mail: songmy@jbnu.ac.kr

is much larger than that of Fe. This led to the reduction of $Fe_2O_3$ and the oxidation of Mg. Most of the researchers studied the effects of metal oxides on the hydrogen release properties of $MgH_2$ in vacuum. On the other hand, in our works we studied the effects of oxide addition on the hydrogen release properties of $MgH_2$ in 1.0 bar $H_2$, which was maintained nearly constant.

Halides have low melting points and milling of Mg or $MgH_2$ with halides may bring about positive effects on the hydrogen uptake and release rates of Mg or $MgH_2$. It is interesting to add halides to Mg to improve the hydrogen storage properties of Mg or $MgH_2$ and to study the phase transition of halides.

Malka et al. [29] milled magnesium hydride with various halides and reported that the best catalysts for magnesium hydride decomposition, among the halides added, were $ZrF_4$, $TaF_5$, $NbF_5$, $VCl_3$ and $TiCl_3$. Seven wt% of various metal halide additives ($ZrF_4$, $TaF_5$, $NbF_5$ and $TiCl_3$) were added to magnesium hydride by ball milling, and the effects of these additives on the hydrogen absorption and release kinetics were investigated by Sieverts' apparatus [30].

4 mol% titanium compounds such as $TiF_3$, $TiCl_3$, $TiO_2$, TiN, or $TiH_2$ were added to $MgH_2$ to catalyzed hydrogen absorption and release kinetics of $MgH_2$ by Ma et al. [31]. $MgH_2$-4 mol% $TiCl_3$ absorbed about 3.7 wt% H at 423 K under a beginning hydrogen pressure of 20 bar and released about 3.85 wt% H at 553 K in a beginning hydrogen pressure of 0.1 bar. In the previous work of our group [32], the hydrogen absorption and release properties of Mg were improved by adding $TiCl_3$ via high-energy ball milling in hydrogen.

In some works, the hydrogen uptake and release rates of magnesium were increased by milling magnesium hydride with metal, compound, or oxide in a planetary mill [18, 20, 27]. Mg is less expensive than $MgH_2$. In this work, we used Mg instead of $MgH_2$ as one of the starting materials.

The optimum content of additives such as transition elements or oxides was about 20 wt% to increase the hydrogen uptake and release rates of magnesium by mechanical grinding under $H_2$ (phase transition-accompanying milling).

In this work, $TiCl_3$ and Ni were chosen as additives to enhance the hydrogen uptake and release rates of Mg. Samples with compositions of 95 wt% Mg+5 wt% $TiCl_3$, 90 wt% Mg+10 wt% $TiCl_3$, and 80 wt% Mg+ 14 wt% Ni+6 wt% $TiCl_3$ were prepared by high-energy ball milling in hydrogen (reactive mechanical grinding, RMG). The previously studied optimum conditions for high-energy ball milling in hydrogen, which is called phase transition-accompanying milling, were used for the sample preparation. The sample was designated as Mg-5$TiCl_3$, Mg-10$TiCl_3$, and Mg-14Ni-6$TiCl_3$, respectively. The hydrogen uptake and release properties of the prepared samples were investigated and compared. The hydrogen storage properties of Mg-14Ni-6$TiCl_3$ were compared with those of $Fe_2O_3$ and Ni-added Mg, which were prepared under the conditions similar to those to prepare Mg-14Ni-6$TiCl_3$.

## Experimental Details

Pure Mg powder (particle size 74-149 μm, purity 99.6%, Alfa Aesar), $TiCl_3$ (Titanium(III) chloride, Aldrich), Ni (average particle size 2.2-3.0 μm, purity 99.9%, Alfa Aesar) were used as the starting materials to prepare samples.

All sample handling was performed in a glove box under Ar in order to prevent oxidation. Mixtures with desired compositions (total weight = 8 g) were milled in a stainless steel container (with 105 hardened steel balls, total weight = 360 g) of a planetary ball mill (Planetary Mono Mill; Pulverisette 6, Fritsch). The disc revolution speed was 250 rpm. The mill container, sealed hermetically, with a volume of 250 ml was filled with high purity hydrogen gas (≈ 12 bar). Milling was performed for 6 h, with hydrogen being refilled every two hours.

The absorbed or released hydrogen quantity was measured as a function of time in nearly constant hydrogen pressures (12 bar $H_2$ for absorption and 1.0 bar $H_2$ for release), using a Sievert's type hydrogen absorption and release apparatus described previously [33]. 0.5 g of the samples was used for these measurements. After the absorbed and then released hydrogen quantities were measured for 1 hr, respectively, the sample was then dehydrided at 623 K in vacuum for 2 hrs. X-ray diffraction (XRD) patterns of the samples after ball milling in hydrogen and after hydrogen uptake-release cycling were obtained with Cu Kα radiation in a Rigaku D/MAX 2500 powder diffractometer. Scanning electron microscope (SEM) micrographs of the samples were obtained by a JSM-5900 SEM operated at 15 kV.

## Results

The percentage of absorbed hydrogen, $H_a$, is expressed with respect to the sample weight. Fig. 1 shows the $H_a$ versus t curves at 593 K in 12 bar $H_2$ at the number of cycles of one (n = 1) for Mg-5$TiCl_3$, Mg-10$TiCl_3$, and Mg-14Ni-6$TiCl_3$. All the samples have quite high initial hydrogen uptake rates and have low hydrogen uptake rates after about 10 min. Mg-5$TiCl_3$ has the highest initial hydrogen uptake rate, followed in a descending order by Mg-10$TiCl_3$ and Mg-14Ni-6$TiCl_3$. Mg-5$TiCl_3$ has the largest quantity of hydrogen absorbed for 60 min, $H_a$ (60 min), followed in a descending order by Mg-10$TiCl_3$ and Mg-14Ni-6$TiCl_3$. Mg-5$TiCl_3$ absorbs 4.84 wt% H for 5 min and 6.27 wt% H for 60 min. Mg-10$TiCl_3$ absorbs 4.06 wt% H for 5 min and 5.59 wt% H for 60 min. Mg-14Ni-

**Table 1.** Variations of $H_a$ at 593 K in 12 bar $H_2$ with time at n = 1 for Mg-5$TiCl_3$, Mg-10$TiCl_3$, and Mg-14Ni-6$TiCl_3$.

| | Absorbed hydrogen quantity (wt% H) | | | | |
|---|---|---|---|---|---|
| | 2.5 min | 5 min | 10 min | 30 min | 60 min |
| Mg-5$TiCl_3$ | 3.54 | 4.84 | 5.86 | 6.24 | 6.27 |
| Mg-10$TiCl_3$ | 3.01 | 4.06 | 5.09 | 5.57 | 5.59 |
| Mg-14Ni-6$TiCl_3$ | 2.83 | 3.96 | 4.51 | 4.95 | 5.03 |

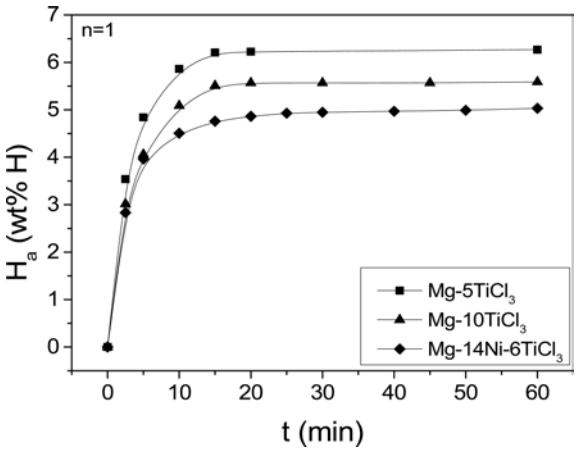


**Fig. 1.** $H_a$ versus t curves at 593 K in 12 bar $H_2$ at n = 1 for Mg-5$TiCl_3$, Mg-10$TiCl_3$, and Mg-14Ni-6$TiCl_3$.

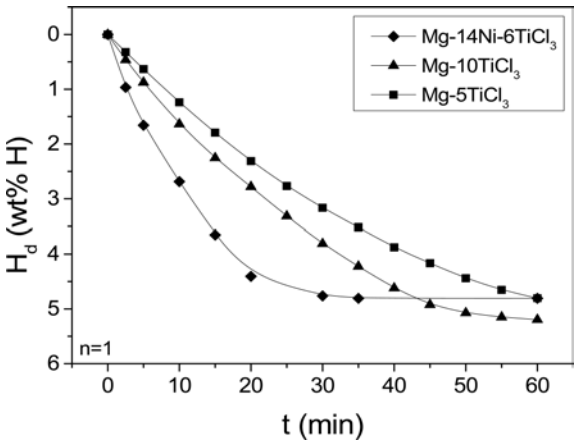


**Fig. 2.** $H_d$ versus t curves at 593 K in 1.0 bar $H_2$ at n = 1 for Mg-5$TiCl_3$, Mg-10$TiCl_3$, and Mg-14Ni-6$TiCl_3$.

6$TiCl_3$ absorbs 3.96 wt% H for 5 min and 5.03 wt% H for 60 min. We define an effective hydrogen storage capacity as a quantity of hydrogen absorbed for 60 min. Mg-5$TiCl_3$ has an effective hydrogen storage capacity of about 6.3 wt% at n = 1. Table 1 gives the variations of $H_a$ at 593 K in 12 bar $H_2$ with time at n = 1 for Mg-5$TiCl_3$, Mg-10$TiCl_3$, and Mg-14Ni-6$TiCl_3$.

The percentage of desorbed (released) hydrogen, $H_d$, is also expressed with respect to the sample weight. The $H_d$ vs. t curves at 593 K in 1.0 bar $H_2$ at n = 1 for Mg-5$TiCl_3$, Mg-10$TiCl_3$, and Mg-14Ni-6$TiCl_3$ are shown in Fig. 2. Mg-14Ni-6$TiCl_3$ has quite high initial

**Table 2.** Variations of $H_d$ at 593 K in 1.0 bar $H_2$ with time at n = 1 for Mg-5$TiCl_3$, Mg-10$TiCl_3$, and Mg-14Ni-6$TiCl_3$.

| | Released hydrogen quantity (wt% H) | | | | |
|---|---|---|---|---|---|
| | 2.5 min | 5 min | 10 min | 30 min | 60 min |
| Mg-5$TiCl_3$ | 0.32 | 0.63 | 1.24 | 3.16 | 4.81 |
| Mg-10$TiCl_3$ | 0.47 | 0.88 | 1.64 | 3.81 | 5.20 |
| Mg-14Ni-6$TiCl_3$ | 0.97 | 1.66 | 2.69 | 4.76 | 4.81 |

**Table 3.** Variations of $H_a$ at 593 K in 12 bar $H_2$ with time at n = 3 for Mg-5$TiCl_3$, Mg-10$TiCl_3$, and Mg-14Ni-6$TiCl_3$.

| | Absorbed hydrogen quantity (wt% H) | | | | |
|---|---|---|---|---|---|
| | 2.5 min | 5 min | 10 min | 30 min | 60 min |
| Mg-5$TiCl_3$ | 3.48 | 4.88 | 5.85 | 6.02 | 6.05 |
| Mg-10$TiCl_3$ | 3.09 | 4.32 | 5.09 | 5.57 | 5.59 |
| Mg-14Ni-6$TiCl_3$ | 3.00 | 4.07 | 5.18 | 5.37 | 5.38 |

**Table 4.** Variations of $H_d$ at 593 K in 1.0 bar $H_2$ with time at n = 3 for Mg-5$TiCl_3$, Mg-10$TiCl_3$, and Mg-14Ni-6$TiCl_3$.

| | Released hydrogen quantity (wt% H) | | | | |
|---|---|---|---|---|---|
| | 2.5 min | 5 min | 10 min | 30 min | 60 min |
| Mg-5$TiCl_3$ | 0.33 | 0.65 | 1.26 | 3.52 | 5.32 |
| Mg-10$TiCl_3$ | 0.38 | 0.74 | 1.46 | 3.70 | 4.98 |
| Mg-14Ni-6$TiCl_3$ | 1.05 | 1.71 | 2.82 | 4.84 | 4.88 |

hydrogen release rate and have low hydrogen release rates after about 20 min. Mg-14Ni-6$TiCl_3$ has the highest initial hydrogen release rate, followed in a descending order by Mg-10$TiCl_3$ and Mg-5$TiCl_3$. Mg-10$TiCl_3$ has the largest quantity of hydrogen released for 60 min, $H_d$ (60 min), followed in a descending order by Mg-14Ni-6$TiCl_3$ and Mg-5$TiCl_3$. Mg-14Ni-6$TiCl_3$ releases 2.69 wt% H for 10 min and 4.76 wt% H for 30 min. Mg-10$TiCl_3$ releases 1.64 wt% H for 10 min and 3.81 wt% H for 30 min. Table 2 gives the variations of $H_d$ at 593 K in 1.0 bar $H_2$ with time at n = 1 for Mg-5$TiCl_3$, Mg-10$TiCl_3$, and Mg-14Ni-6$TiCl_3$.

The activation of Mg-5$TiCl_3$, Mg-10$TiCl_3$, and Mg-14Ni-6$TiCl_3$ was completed after three hydrogen uptake-release cycles. Fig. 3 shows the $H_a$ versus t curves at 593 K in 12 bar $H_2$ at n = 3 for Mg-5$TiCl_3$, Mg-10$TiCl_3$, and Mg-14Ni-6$TiCl_3$. All the samples have quite high initial hydrogen uptake rates and have low hydrogen uptake rates after about 10 min. Mg-5$TiCl_3$ has the highest initial hydrogen uptake rate, followed in a descending order by Mg-10$TiCl_3$ and Mg-14Ni-6$TiCl_3$. Mg-5$TiCl_3$ has the largest quantity of hydrogen absorbed for 60 min, $H_a$ (60 min), followed in a descending order by Mg-10$TiCl_3$ and Mg-14Ni-6$TiCl_3$. Mg-5$TiCl_3$ absorbs 5.06 wt% H for 5 min and 6.19 wt% H for 60 min. Mg-10$TiCl_3$ absorbs 4.32 wt% H for 5 min and 5.38 wt% H for 60 min. Mg-14Ni-6$TiCl_3$ absorbs 4.07 wt% H for 5 min and 5.20 wt% H for 60 min. Table 3 gives the variations of $H_a$ at 593 K in 12 bar $H_2$ with time at

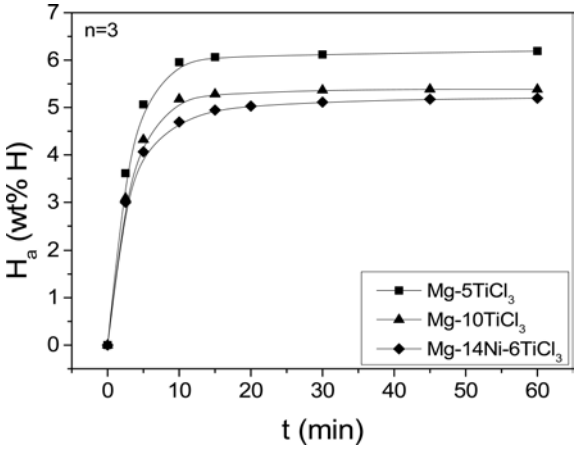


**Fig. 3.** $H_a$ versus t curves at n = 3 at 593K in 12 bar $H_2$ for Mg-5TiCl$_3$, Mg-10TiCl$_3$, Mg-14Ni-6TiCl$_3$.

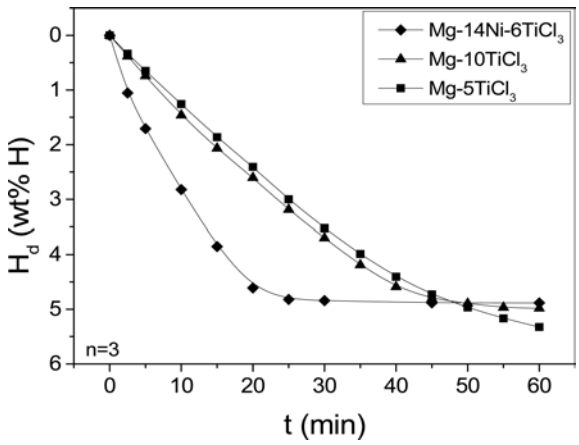


**Fig. 4.** $H_d$ versus t curves at n = 3 at 593K in 1.0 bar $H_2$ for Mg-5TiCl$_3$, Mg-10TiCl$_3$, Mg-14Ni-6TiCl$_3$.

n = 3 for Mg-5TiCl$_3$, Mg-10TiCl$_3$, and Mg-14Ni-6TiCl$_3$.

The $H_d$ vs. t curves at 593 K in 1.0 bar $H_2$ at n = 3 for Mg-5TiCl$_3$, Mg-10TiCl$_3$, and Mg-14Ni-6TiCl$_3$ are shown in Fig. 4. Mg-14Ni-6TiCl$_3$ has quite high initial hydrogen release rate and have low hydrogen release rates after about 20 min. Mg-14Ni-6TiCl$_3$ has the highest initial hydrogen release rate, followed in a descending order by Mg-10TiCl$_3$ and Mg-5TiCl$_3$. Mg-5TiCl$_3$ has the largest quantity of hydrogen released for 60 min, $H_d$ (60 min), followed in a descending order by Mg-10TiCl$_3$ and Mg-14Ni-6TiCl$_3$. Mg-14Ni-6TiCl$_3$ releases 2.82 wt% H for 10 min and 4.84 wt% H for 30 min. Mg-10TiCl$_3$ releases 1.46 wt% H for 10 min and 3.70 wt% H for 30 min. Table 4 gives the variations of $H_d$ at 593 K in 1.0 bar $H_2$ with time at n = 3 for Mg-5TiCl$_3$, Mg-10TiCl$_3$, and Mg-14Ni-6TiCl$_3$.

Fig. 5 exhibits the microstructures of Mg-5TiCl$_3$, Mg-10TiCl$_3$, and Mg-14Ni-6TiCl$_3$ after reactive mechanical grinding. The particle sizes are not homogeneous and the shapes of particles are irregular. Mg-10TiCl$_3$ has smaller particles than Mg-5TiCl$_3$ and the particles of Mg-14Ni-6TiCl$_3$ are much larger than Mg-5TiCl$_3$ and Mg-10TiCl$_3$.

The particles of Mg-5TiCl$_3$, Mg-10TiCl$_3$, and Mg-14Ni-6TiCl$_3$ dehydrided at the 4$^{th}$ hydrogen uptake-release cycle were agglomerated and the particles on the surfaces of the agglomerates were fine. The agglomeration of particles is partly due to the maintenance of the samples at relatively high temperature during hydrogen uptake-release cycling and the formation of fine particles on the surfaces of the agglomerates is owing to expansion by hydrogen uptake reaction and contraction by hydrogen release reaction of particles.

Fig. 6 shows the particle size distributions of Mg-5TiCl$_3$, Mg-10TiCl$_3$, and Mg-14Ni-6TiCl$_3$ after reactive mechanical grinding. Mg-5TiCl$_3$ has the highest particle percent peak at a particle diameter of about 0.015 μm, followed in order by those at particle diameters of about 0.4 μm and 1.7 μm. Mg-10TiCl$_3$ has a particle percent peak at a particle diameter of about 0.015 μm. Mg-14Ni-6TiCl$_3$ has a particle percent peak at a particle diameter of about 0.25 μm. Mg-10TiCl$_3$ has the smallest average particle size (0.01 μm), followed in order by Mg-5TiCl$_3$ (0.20 μm) and Mg-14Ni-6TiCl$_3$ (0.41 μm), corresponding well to the microstructures shown in Fig. 5.

The particle size distributions of Mg-5TiCl$_3$, Mg-10TiCl$_3$, and Mg-14Ni-6TiCl$_3$ dehydrided at the 4$^{th}$ hydrogen uptake-release cycle are presented in Fig. 7. Three samples have a particle percent peak at a particle diameter of about 0.02 μm. The average particle sizes

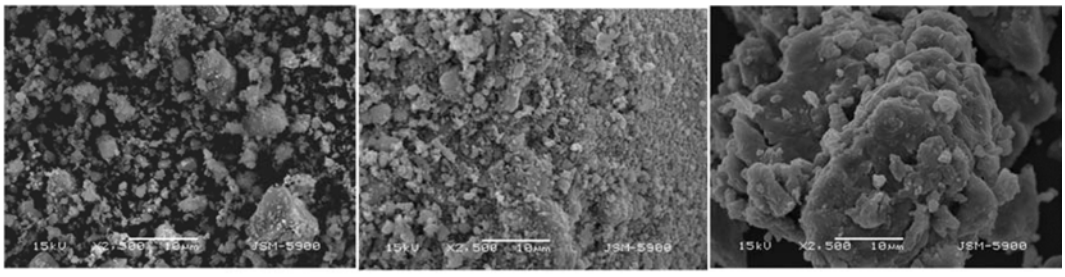


**Fig. 5.** Microstructures of (a) Mg-5TiCl$_3$, (b) Mg-10TiCl$_3$, and (c) Mg-14Ni-6TiCl$_3$ after reactive mechanical grinding.

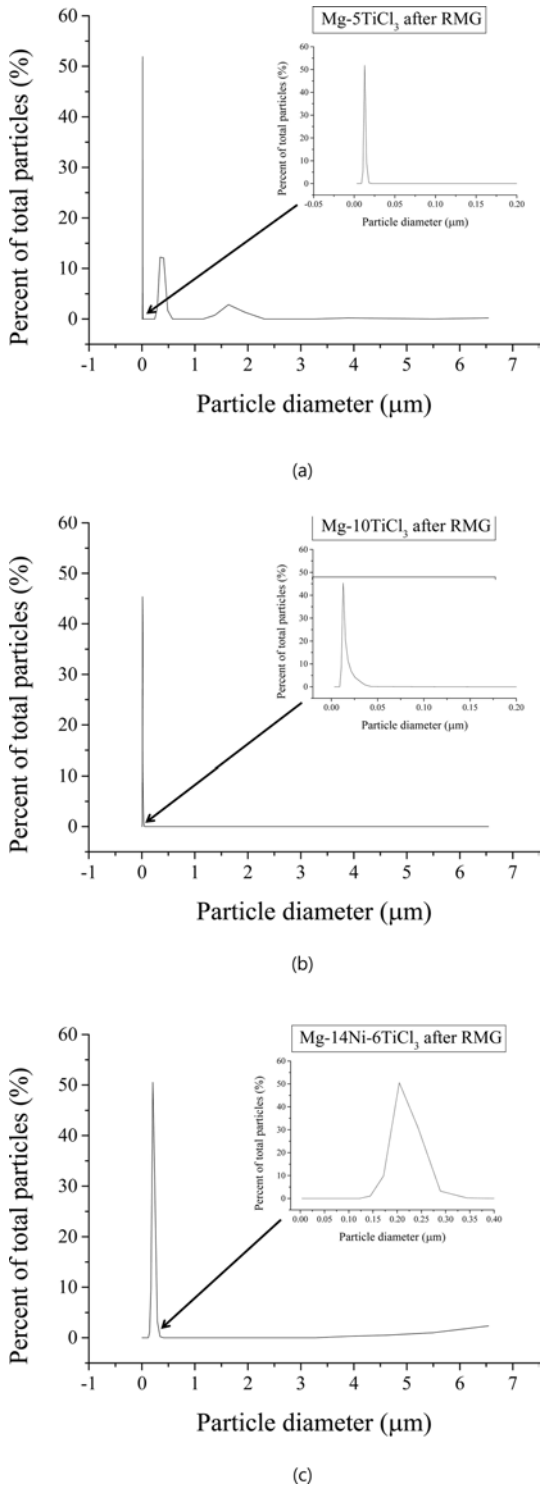


**Fig. 6.** Particle size distributions of (a) Mg-5$TiCl_3$, (b) Mg-10$TiCl_3$, and (c) Mg-14Ni-6$TiCl_3$ after reactive mechanical grinding.

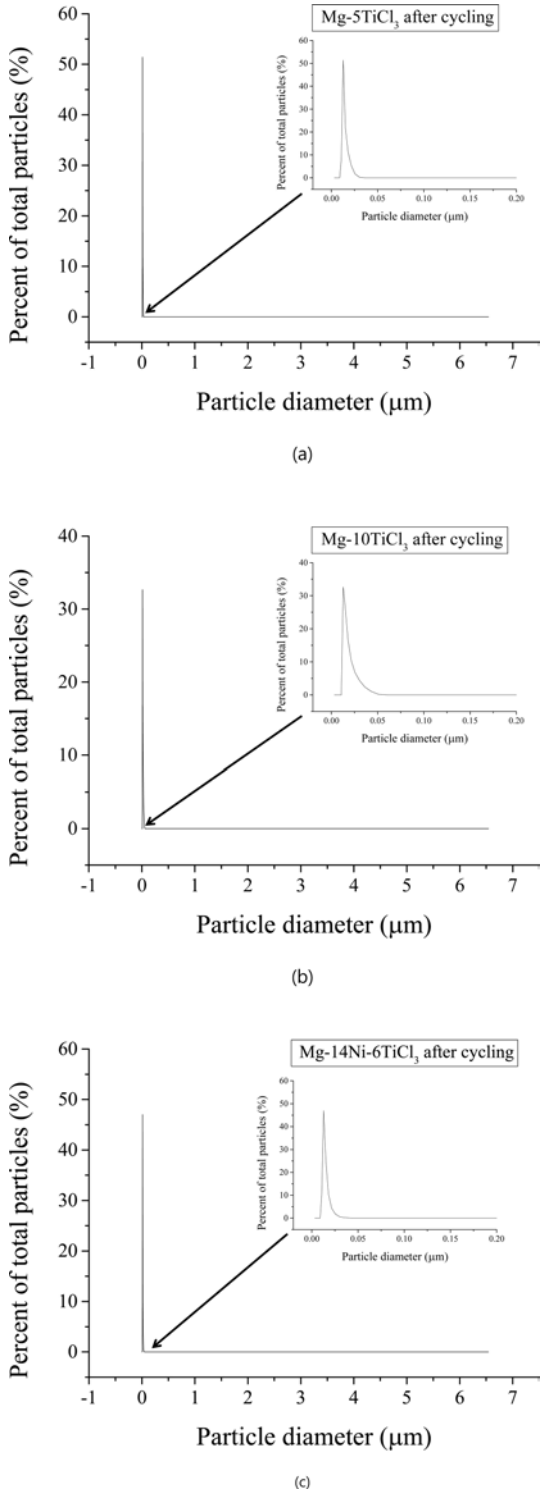


**Fig. 7.** Particle size distributions of (a) Mg-5$TiCl_3$, (b) Mg-10$TiCl_3$, and (c) Mg-14Ni-6$TiCl_3$ dehydrided at the 4$^{th}$ hydrogen uptake-release cycle.

of Mg-5$TiCl_3$ (0.01 μm), Mg-10$TiCl_3$ (0.02 μm), and Mg-14Ni-6$TiCl_3$ (0.01 μm) are very similar. This coincides well with the microstructures of Mg-5$TiCl_3$, Mg-10$TiCl_3$, and Mg-14Ni-6$TiCl_3$ dehydrided at the 4$^{th}$ hydrogen uptake-release cycle.

Fig. 8 presents the XRD pattern of Mg-14Ni-6$TiCl_3$ dehydrided at the 4$^{th}$ hydrogen uptake-release cycle. The sample contains Mg, $Mg_2Ni$, MgO, β-$MgH_2$, and a small amount of $TiH_{1.924}$. The $Mg_2Ni$ phase, which was not observed after milling, is observed in the sample dehydrided after cycling. $TiH_{1.924}$ observed in the sample

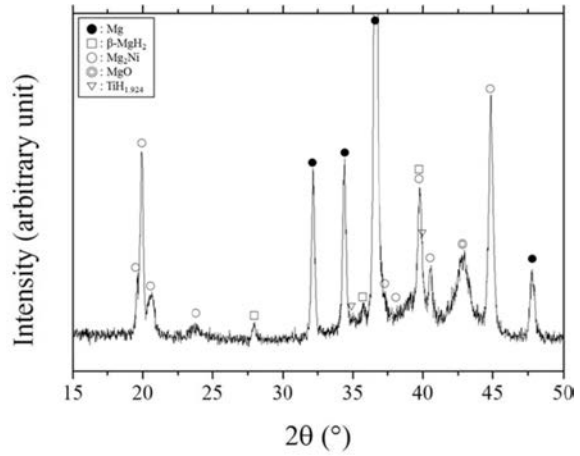


**Fig. 8.** XRD pattern of Mg-14Ni-6$TiCl_3$ dehydrided at the 4th hydrogen uptake-release cycle.

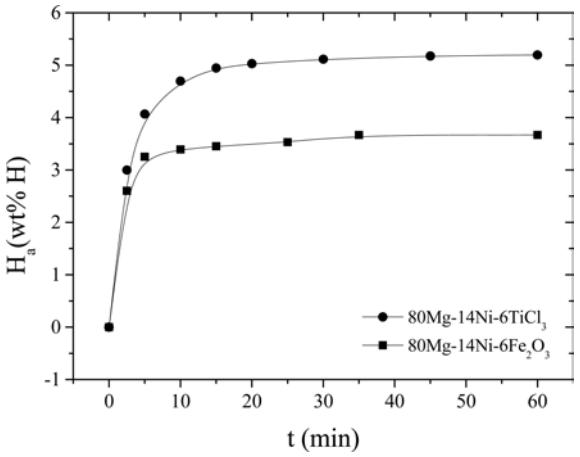


**Fig. 9.** Ha vs. t curves at 593 K under 12 bar $H_2$ at n = 3 for Mg-14Ni-6$TiCl_3$ and Mg-14Ni-6$Fe_2O_3$.

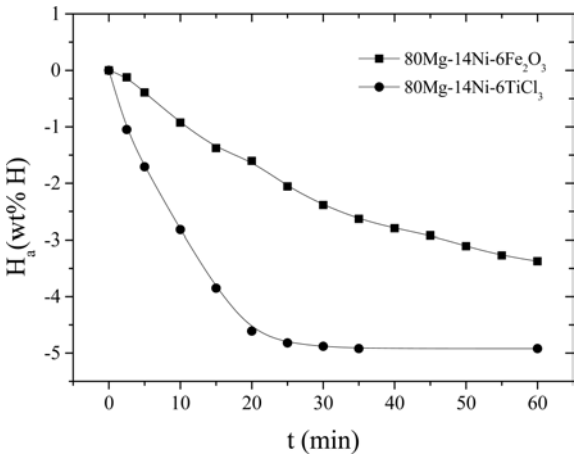


**Fig. 10.** Hd vs. t curves at 593 K under 1.0 bar $H_2$ at n = 3 for Mg-14Ni-6$TiCl_3$ and Mg-14Ni-6$Fe_2O_3$.

after phase transition-accompanying milling remains undecomposed.

Fig. 9 shows the $H_a$ vs. t curves at 593 K under 12 bar $H_2$ at n = 3 for Mg-14Ni-6$TiCl_3$ and Mg-14Ni-6$Fe_2O_3$ [34]. Both of the samples have quite high initial hydrogen uptake rates and have low hydrogen uptake rates after about 10 min. Mg-14Ni-6$TiCl_3$ has a higher initial hydrogen uptake rate than Mg-14Ni-6$Fe_2O_3$. Mg-14Ni-6$TiCl_3$ has a larger quantity of hydrogen absorbed for 60 min, $H_a$ (60 min), than Mg-14Ni-6$Fe_2O_3$. Mg-14Ni-6$TiCl_3$ absorbs 3.00 wt% H for 2.5 min and 5.20 wt% H for 60 min. Table 5 shows the variations of $H_a$ at 593 K under 12 bar $H_2$ with time at n = 3 for Mg-14Ni-6$TiCl_3$ and Mg-14Ni-6$Fe_2O_3$.

The $H_d$ vs. t curves at 593 K under 1.0 bar $H_2$ at n = 3 for Mg-14Ni-6$TiCl_3$ and Mg-14Ni-6$Fe_2O_3$ [34] are shown in Fig. 10. Mg-14Ni-6$TiCl_3$ and Mg-14Ni-3$Fe_2O_3$-3Ti have quite high initial hydrogen release rates and have low hydrogen release rates after about 20 min. Mg-14Ni-6$TiCl_3$ has a higher initial hydrogen release rate than Mg-14Ni-6$Fe_2O_3$. Mg-14Ni-6$TiCl_3$ has a larger quantity of hydrogen released for 60 min, $H_d$ (60 min), than Mg-14Ni-6$Fe_2O_3$. Mg-14Ni-6$TiCl_3$ releases 2.82 wt% H for 10 min antid 4.84 wt% H for 30 min. Table 6 shows the variaons of $H_d$ at 593 K under 1.0 bar $H_2$ with time at n = 3 for Mg-14Ni-6$TiCl_3$ and Mg-14Ni-6$Fe_2O_3$.

## Discussion

The $Mg_2Ni$ phase forms its hydride ($Mg_2NiH_4$) under similar conditions for hydrogen uptake reaction of Mg and $Mg_2NiH_4$ releases hydrogen under similar conditions for hydrogen release reaction of $MgH_2$ [2]. $Mg_2Ni$ has higher hydrogen uptake and release rates than Mg. $TiH_{1.924}$ observed in the sample after phase transition-accompanying milling remains undecomposed. During hydrogen uptake-release cycling, the hydrogen uptake and release reactions of Mg and $Mg_2Ni$ occur. During hydrogen uptake-release cycling, the hydrogen uptake and release reactions of Mg and $Mg_2Ni$ occur.

Fig. 1 shows that all the samples have quite high initial hydrogen uptake rates. This shows that the nucleation of the hydride phases occurs rapidly, i.e. the nucleation of the hydride phases is not a rate-controlling step. Fig. 1 shows that Mg-5$TiCl_3$ has the highest initial hydrogen uptake rate and the largest $H_a$ (60 min), followed in a descending order by Mg-10$TiCl_3$ and Mg-14Ni-6$TiCl_3$. Decrease of the Mg proportion in Mg-10$TiCl_3$, compared with that in Mg-5$TiCl_3$, is thought to decrease the initial hydrogen uptake rate and the quantity of hydrogen absorbed for 60 min. Ni in Mg-14Ni-6$TiCl_3$ forms $Mg_2Ni$, having a lower hydrogen-storage capacity than Mg, by a reaction with Mg after hydrogen uptake-release cycling. Decrease in the Mg proportion in Mg-14Ni-6$TiCl_3$, compared with those in Mg-5$TiCl_3$ and Mg-10$TiCl_3$, and the formation of $Mg_2Ni$, with a lower hydrogen storage capacity than Mg, are thought to decrease the initial hydrogen uptake rate and the quantity

**Table 5.** Variations of $H_a$ (wt% H) at 593 K under 12 bar $H_2$ with time at n = 3 for Mg-14Ni-6$TiCl_3$ and Mg-14Ni-6$Fe_2O_3$.

| | 2.5 min | 5 min | 10 min | 60 min |
|---|---|---|---|---|
| Mg-14Ni-6$TiCl_3$ | 3.00 | 4.07 | 5.18 | 5.38 |
| Mg-14Ni-6$Fe_2O_3$ | 2.60 | 3.25 | 3.39 | 3.67 |

**Table 6.** Variations of $H_d$ (wt% H) at 593 K under 1.0 bar $H_2$ with time at n = 3 for Mg-14Ni-6$TiCl_3$ and Mg-14Ni-6$Fe_2O_3$.

| | 2.5 min | 5 min | 10 min | 30 min |
|---|---|---|---|---|
| Mg-14Ni-6$TiCl_3$ | 1.05 | 1.71 | 2.82 | 4.84 |
| Mg-14Ni-6$Fe_2O_3$ | 0.12 | 0.39 | 0.93 | 2.39 |

of hydrogen absorbed for 60 min for Mg-14Ni-6$TiCl_3$.

Comparison of Fig. 3 with Fig. 1 shows that as the number of cycles increases from one to three, the initial hydrogen uptake rates of all the samples increase, while the $H_a$ (60 min)'s of Mg-5$TiCl_3$ and Mg-10$TiCl_3$ decrease and the $H_a$ (60 min) of Mg-14Ni-6$TiCl_3$ increases. Expansion by hydrogen uptake reaction and contraction by hydrogen release reaction of particles during hydrogen uptake-release cycling decrease the size of the particles on the surfaces of agglomerates, increasing the initial hydrogen uptake rates of all the samples [35-40]. Due to maintenance at a relatively high temperature coalesce the cracks in the interior of the particles of Mg-5$TiCl_3$ and Mg-10$TiCl_3$, decreasing the $H_a$ (60 min)'s of Mg-5$TiCl_3$ and Mg-10$TiCl_3$. However, the phases formed such as $Mg_2Ni$ and $TiH_{1.924}$ in Mg-14Ni-6$TiCl_3$ prevents the coalescence of the cracks in the interior of particles of Mg-14Ni-6$TiCl_3$ even though the samples is maintained a relatively high temperature, increasing slightly the $H_a$ (60 min) of Mg-14Ni-6$TiCl_3$ (since the effect of expansion and contraction predominates).

Fig. 2 shows that at n = 1, Mg-14Ni-6$TiCl_3$ has the highest initial hydrogen release rate, followed in a descending order by Mg-10$TiCl_3$ and Mg-5$TiCl_3$. Fig. 4 also shows that at n = 3, Mg-14Ni-6$TiCl_3$ has the highest initial hydrogen release rate, followed in a descending order by Mg-10$TiCl_3$ and Mg-5$TiCl_3$, the initial hydrogen release rate of Mg-5$TiCl_3$ approaching that of Mg-10$TiCl_3$.

The equilibrium plateau pressure in the Mg-H system at 593 K is reportedly 2.70 bar [41]. The driving force for the hydrogen uptake reaction (the applied hydrogen pressure – the equilibrium plateau pressure) of Mg-5$TiCl_3$ is 9.30 bar $H_2$ while that for the hydrogen release reaction (the equilibrium plateau pressure-the applied hydrogen pressure) of Mg-5$TiCl_3$ is 1.70 bar $H_2$. The hydrogen uptake rate of Mg-5$TiCl_3$ at 593K in 12 bar $H_2$ at n = 1 (the average hydrogen uptake rate for 5 min = 0.97 wt% H/min) is much higher than the hydrogen release rate of Mg-5$TiCl_3$ at 593K under 1.0 bar $H_2$ at n = 1 (the average hydrogen release rate for 5 min = 0.13 wt% H/min). The difference in the driving forces led to this result. Due to the small driving force for hydrogen release reaction, the rate-controlling step for the hydrogen release reaction of the hydrided Mg-5$TiCl_3$, Mg-10$TiCl_3$, and Mg-14Ni-6$TiCl_3$ is believed to be the nucleation of Mg-H solid solution (The main phase in the hydrided Mg-5$TiCl_3$ is Mg hydride). The larger content of $TiCl_3$ in Mg-10$TiCl_3$ favors the nucleation of Mg-H solid solution, compared to that in Mg-5$TiCl_3$ since the additive can act as active sites for the nucleation of Mg-H solid solution. This leads to the higher initial hydrogen release rate in Mg-10$TiCl_3$ than in Mg-5$TiCl_3$.

Fig. 8 shows that $Mg_2Ni$ phase forms after hydrogen uptake-release cycling. $Mg_2Ni$ has higher hydrogen uptake and release rates than Mg [3]. The rate-controlling step for the hydrogen release reaction of a mechanically alloyed mixture Mg-10 wt% Ni was reported to be both the bulk and Knudsen flow of hydrogen gas [42]. The rapid decomposition of $Mg_2Ni$ hydride will provide passages for gas phase mass transfer of hydrogen from Mg hydride. In addition, the decomposed $Mg_2Ni$ hydride may act as active sites for the Mg-H nucleation. The $Mg_2Ni$ formed in Mg-14Ni-6$TiCl_3$ and the larger content of additives (favoring the nucleation of Mg-H solid solution) are believed to increase the hydrogen release rate of Mg-14Ni-6$TiCl_3$, making Mg-14Ni-6$TiCl_3$ have the highest initial hydrogen release rate among these three samples.

Fig. 2 shows that Mg-10$TiCl_3$ has the largest quantity of hydrogen released for 60 min, $H_d$ (60 min), followed in a descending order by Mg-14Ni-6$TiCl_3$ and Mg-5$TiCl_3$. However, the trends of the $H_d$ vs. t curves for the three samples suggest that Mg-5$TiCl_3$ has the largest quantity of hydrogen released for a longer time, for example, 90 min, followed in a descending order by Mg-10$TiCl_3$ and Mg-14Ni-6$TiCl_3$. Fig. 4 shows that Mg-5$TiCl_3$ has the largest quantity of hydrogen released for 60 min, $H_d$ (60 min), followed in a descending order by Mg-10$TiCl_3$ and Mg-14Ni-6$TiCl_3$. Decrease in the Mg proportion in Mg-10$TiCl_3$, compared with that in Mg-5$TiCl_3$, is thought to decrease the quantity of hydrogen released for 60 min. Ni in Mg-14Ni-6$TiCl_3$ forms $Mg_2Ni$, having a lower hydrogen-storage capacity than Mg, by a reaction with Mg after hydrogen uptake-release cycling. Decrease in the Mg proportion in Mg-14Ni-6$TiCl_3$, compared with those in Mg-5$TiCl_3$ and Mg-10$TiCl_3$, and the formation of $Mg_2Ni$, with a lower hydrogen storage capacity than Mg, are thought to decrease the quantity of hydrogen released for 60 min for Mg-14Ni-6$TiCl_3$.

Comparison of Fig. 4 with Fig. 2 shows that as the number of cycles increases from one to three, the initial hydrogen release rate and the $H_a$ (60 min) of Mg-14Ni-6$TiCl_3$ increase slightly. As the number of cycles increases from n = 1 to n = 3, the initial hydrogen release rate of Mg-5$TiCl_3$ increases slightly and the $H_a$ (60 min) of Mg-5$TiCl_3$ increase while those of Mg-

$10TiCl_3$ decrease. It is believed that the larger content of $TiCl_3$ in Mg-$10TiCl_3$ makes the nucleation of Mg-H solid solution easy, leading to a higher initial hydrogen release rate in Mg-$10TiCl_3$ than in Mg-$5TiCl_3$. The hydrogen uptake-release cycling brings about the creation of defects, which can act active nucleation sites, and the decrease in particle size. However, the effects of maintenance in a relatively high temperature, 593 K, are believed to decrease the number of defects and to increase the particle size [43-48]. It is thought that in Mg-$5TiCl_3$, the effects of the hydrogen uptake-release cycling are stronger than those of maintenance in a relatively high temperature while in Mg-$10TiCl_3$, the effects of maintenance in a relatively high temperature are stronger than those of the hydrogen uptake-release cycling. This leads to the increases in the initial hydrogen release rate and the $H_d$ (60 min) in Mg-$5TiCl_3$, contradistinctively to the decreases in the initial hydrogen release rate and the $H_d$ (60 min) in Mg-$10TiCl_3$.

By considering the initial hydrogen uptake rate, $H_a$ (60 min), the initial hydrogen release rate, $H_d$ (60 min), and the cycling performance, Mg-14Ni-$6TiCl_3$ is thought to be the best hydrogen-storage material among these three samples.

## Conclusions

Mg-$5TiCl_3$, Mg-$10TiCl_3$, and Mg-14Ni-$6TiCl_3$ samples were prepared by high-energy ball milling in hydrogen. At the first cycle (n = 1), Mg-$5TiCl_3$ had the highest initial hydrogen uptake rate and the largest $H_a$ (60 min) at 593 K in 12 bar $H_2$, followed in a descending order by Mg-$10TiCl_3$ and Mg-14Ni-$6TiCl_3$. Mg-$5TiCl_3$ had an effective hydrogen storage capacity of about 6.3 wt% at n = 1. Mg-14Ni-$6TiCl_3$ absorbed 3.96 wt% H for 5 min and 5.03 wt% H for 60 min. At n = 1, Mg-14Ni-$6TiCl_3$ has the highest initial hydrogen release rate at 593 K in 1.0 bar $H_2$. Due to the small driving force for hydrogen release reaction, the rate-controlling step for the hydrogen release reaction of the three hydrided samples is believed to be the nucleation of Mg-H solid solution. The larger content of $TiCl_3$ favors the nucleation of Mg-H solid solution since the additive can act as active sites for the nucleation of Mg-H solid solution. The $Mg_2Ni$ formed in Mg-14Ni-$6TiCl_3$ and the larger content of additives (favoring the nucleation of Mg-H solid solution) are believed to increase the hydrogen release rate of Mg-14Ni-$6TiCl_3$, making Mg-14Ni-$6TiCl_3$ have the highest initial hydrogen release rate among the three samples. Mg-14Ni-$6TiCl_3$ had a higher initial hydrogen uptake rate, $H_a$ (60 min), a higher initial hydrogen release rate, and $H_d$ (30 min) than $Fe_2O_3$ and Ni-added Mg samples.

## Acknowledgements

This research was supported by Basic Science Research Program through the National Research Foundation (NRF) of Korea funded by the Ministry of Education, Science and Technology (grant number 2011-0023566). This paper was supported by the selection of research-oriented professor of Chonbuk National University in 2019.

## References

1. J.J. Reilly and R.H. Wiswall, Inorg. Chem. 6[12] (1967) 2220 -2223.
2. J.J. Reilly and R.H. Wiswall Jr, Inorg. Chem. 7[11] (1968) 2254-2256.
3. E. Akiba, K. Nomura, S. Ono and S. Suda, Int. J. Hydrogen Energy 7[10] (1982) 787-791.
4. S. Ogawa, T. Fujimoto, T. Mizutani, M. Ogawa, S. Yagi, Int. J. Hydrogen Energy 40[35] (2015) 11895-901.
5. D. Wu, L. Ouyang, C. Wu, H. Wang, M. Zhu, J. Alloys Compd. 642 (2015) 180-184.
6. G.H. Ağaoğlu, G. Orhan, Int. J. Hydrogen Energy 42[12] (2017) 8098-8108.
7. M. Calizzi, D. Chericoni, L.H. Jepsen, T.R. Jensen, L. Pasquini, Int. J. Hydrogen Energy 41[32] (2016) 14447-14454.
8. L. Xie, J. Li, T. Zhang, H. Kou, Renewable Energy 113 (2017) 1399-1407.
9. K.L. Lim, Y. Liu, Q.-A. Zhang, K.-S. Lin, S.L.I. Chan, Int. J. Hydrogen Energy 42[37] (2017) 23737-23745.
10. J. Hu, M. Fichtner, M. Baricco, Int. J. Hydrogen Energy 42[27] (2017) 17144-17148.
11. B. Zhang, Y. Lv, J. Yuan, Y. Wu, J. Alloys Compd. 702 (2017) 126-131.
12. S. Agarwal, A. Jain, P. Jain, M. Jangir, I.P. Jain, J. Alloys Compd. 645 (Supplement 1) (2015) S518-523.
13. M.Y. Song, J. Mater. Sci. 30 (1995) 1343-1351.
14. M.Y. Song, E.I. Ivanov, B. Darriet, M. Pezat, P. Hagenmuller, Int. J. Hydrogen Energy 10 (1985) 169-178.
15. M.Y. Song, E.I. Ivanov, B. Darriet, M. Pezat, P. Hagenmuller, J. Less-Common Met. 131 (1987) 71-79.
16. M.Y. Song, Int. J. Hydrogen Energy 28 (2003) 403-408.
17. J.-L. Bobet, E. Akiba, Y. Nakamura, B. Darriet, Int. J. Hydrogen Energy 25 (2000) 987-996.
18. W. Oelerich, T. Klassen, R. Bormann, J. Alloys Compd. 322 (2001) L5-9.
19. W. Oelerich, T. Klassen, R. Bormann, J. Alloys Compd. 315 (2001) 237-242.
20. Z. Dehouche, T. Klassen, W. Oelerich, J. Goyette, T.K. Bose, R. Schulz, J. Alloys Compd. 347 (2002) 319-323.
21. M.Y. Song, J-L. Bobet. B. Darriet, J. Alloys Compd. 340 (2002) 256-262.
22. J.-L. Bobet, F.J. Castro, B. Chevalier, Scripta Materialia 52 (2005) 33-37.
23. K.S. Jung, E.Y. Lee, K.S. Lee, J. Alloys Compd. 421 (2006) 179-184.
24. M.Y. Song, S.N. Kwon, D.R. Mumm, and S.-H. Hong, Curr. App. Phys. 9 (2009) S118-120.
25. K.-F. Aguey-Zinsou, T. Nicolaisen, J.R. Ares Fernandez, T. Klassen, R. Bormann, J. Alloys Compd. 434-435 (2007) 738-742.
26. R. Gupta, F. Agresti, S. Lo Russo, A. Maddalena, P. Palade,

G. Principi, J. Alloys Compd. 450 (2008) 310-313.
27. G. Barkhordarian, T. Klassen, R. Bormann, Scripta Materialia 49 (2003) 213–217.
28. O. Friedrichs, T. Klassen, J.C. Sánchez-López, R. Bormann and A. Fernández, Scripta Materialia 54[7] (2006) 1293-1297.
29. I.E. Malka, T. Czujko, J. Bystrzycki, Int. J. Hydrogen Energy 35 (2010) 1706-1712.
30. I.E. Malka, M. Pisarek, T. Czujko, J. Bystrzycki, Int. J. Hydrogen Energy 36 (2011) 12909-12917.
31. L.-P. Ma, P. Wang, H.-M. Cheng, Int. J. Hydrogen Energy 35 (2010) 3046-3050.
32. S.H. Lee, Y.J. Kwak, H.R. Park, M.Y. Song, Korean J. Met. Mater. 53 (2015) 187-192.
33. M.Y. Song, S.H. Baek, J.-L. Bobet, S.H. Hong, Int. J. Hydrogen Energy 35 (2010) 10366-10372.
34. Y.J. Kwak, Effects of Ni, $Fe_2O_3$, Ti, and Fe Addition by Reactive Mechanical Grinding on the Hydrogen Storage Characteristics of Mg, M.E. thesis, Chonbuk National University, (2012).
35. H.R. Park, Y.J. Kwak, M.Y. Song, Korean J. Met. Mater. 55 (2017) 656-662.
36. S.-H. Hong, Y.J. Kwak, M.Y. Song, Korean J. Met. Mater. 56 (2018) 59-65.
37. S.-H. Hong, M.Y. Song, Korean J. Met. Mater. 56 (2018) 155-162.
38. Y.J. Kwak, H.R. Park, M.Y. Song, Met. Mater. Int. 22 (2018) 423-432.
39. M.Y. Song, E. Choi, Y.J. Kwak, Korean J. Met. Mater. 56 (2018) 392-399.
40. M.Y. Song, Y.J. Kwak, E. Choi, Korean J. Met. Mater. 56 (2018) 524-531.
41. Y.J. Kwak, M.Y. Song, Korean J. Met. Mater. 56 (2018) 244-251.
42. M.Y. Song, J.-P. Manaud, B. Darriet, J. Alloys Compd. 282(1999) 243-247
43. Y.J. Kwak, E. Choi, M.Y. Song, Met. Mater. Int. 24 (2018) 1181-1190.
44. M.Y. Song, Y.J. Kwak, Korean J. Met. Mater. 56 (2018) 611-619.
45. E. Choi, Y.J. Kwak, M.Y. Song, Met. Mater. Int. 24 (2018) 1403-1411.
46. M.Y. Song, E. Choi, Y.J. Kwak, Korean J. Met. Mater. 56 (2018) 620-627.
47. M.Y. Song, Y.J. Kwak, Korean J. Met. Mater. 56 (2018) 878-884.
48. Y.J. Kwak, M.Y. Song, Nanosci. Nanotech. Lett. 10(5) (2018) 772-778.